Optical Beam Control Testbeds

Brij. N. Agrawal[1]
Naval Postgraduate School, Monterey, CA, 93943

and

Ty Martinez[2]
Naval Research Laboratory, Albuquerque, NM , 87177

This paper discusses two optical beam control testbeds developed at the Spacecraft Research and Design Center, Naval Postgraduate School, to evaluate and develop control techniques for jitter and adaptive optics control. The first testbed, a Jitter Control Testbed is used to develop control techniques for optical beam jitter. In the second testbed, the Adaptive Optics Testbed, adaptive optics control techniques are used to control the surfaces of a segmented mirror with the objective of minimizing aberrations in the images. This paper will also discuss the evaluation of different control techniques used in jitter and adaptive optics control.

I.   Introduction

In a number of applications, such as imaging , laser communications, and high energy lasers, there are challenging requirements for jitter control and wavefront error minimization. For some future space missions, the problem becomes more difficult because of the use of large flexible segmented mirrors and complex optical systems, such as in the James Webb Space Telescope. In the past, classical PID (position, integral and derivative) control has been used. However, these methods are not able to meet performance requirements for large complex flexible optical systems. Consequently, the application and evaluation of modern control techniques will be necessary. For adaptive optics, there are hundreds of sensors and actuators which are likely coupled. Consequently, Single Input Single Output classical control techniques may not be adequate. In these cases, a Multi-Input Multi-Output approach using robust control techniques may be required. Therefore, optical beam control is a challenging problem for the control engineer.

On a program with tight funding and a short schedule, it is expensive and time consuming to evaluate different control techniques. This can result in the use of well-proven classical control techniques at the expense of performance, which could be improved with the use of more modern techniques. Different control techniques, however, can be evaluated on testbeds cost-effectively, simulating some basic components of the system and providing higher confidence in application of these techniques on flight systems. The Spacecraft Research and Design Center, at the Naval Postgraduate School has constructed two such testbeds for the purpose of developing and evaluating control techniques for jitter and adaptive optics control.

The jitter control testbed investigates different control algorithms to remove disturbance jitter with Fast Steering Mirrors (FSMs). For spacecraft applications, jitter is caused by various elements including solar arrays, reaction wheels, control moment gyroscopes and payloads with structural control interactions. Using this testbed, various control algorithms for jitter control were implemented including a Least Mean Square (LMS) algorithm[1] and adaptive and feedback control methods[2]. Recently, an adaptive Recursive Least Square (RLS) algorithm was successfully implemented on the testbed to provide further improvement in the control design[3].

The adaptive optics testbed is designed to correct aberrations in an optical wavefront in addition to removing jitter. The aberrations in the wavefront can be caused from various sources such as imperfections in the optical elements, atmospheric disturbances, structural deformation of optical elements, etc. Because of the weight constraints for space-based optics systems, the optical system elements will likely be light and flexible, and the

---

[1] Distinguished Professor, Department of Astronautical Engineering, Naval Postgraduate School ME/Ag, AIAA Associate Follow.
[2]Research Scientist, Naval Research Laboratory.

shape control of the mirror surface becomes a challenging task. The adaptive optics testbed successfully demonstrated phase estimation and control techniques previously available in the literature[4]. In this paper, we present the details and operational results of both testbeds.

II. Laser Jitter Control Testbed

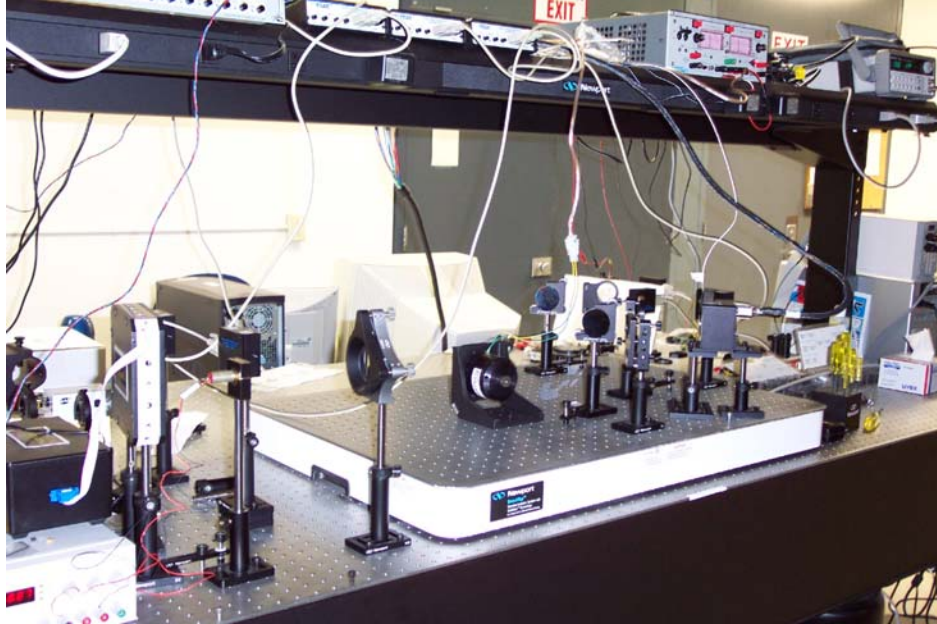### A. Testbed Description

Figure 1. Laser jitter control testbed

To develop improved techniques for optical beam jitter control, a Laser Jitter Control (LJC) Testbed was developed at the Naval Postgraduate School as shown in Fig 1 and Fig 2. The components are mounted on a Newport optical bench, which can be floated to isolate the components from external vibrations. The laser beam originates from a source and passes through a Disturbance Injection Fast Steering Mirror (DFSM). The DFSM corrupts the beam using random or periodic disturbances simulating disturbances that might originate with the transmitting station or tip and tilt errors which the beam may suffer as it passes through the atmosphere. A vibration isolation platform is used to mount the relay system and to isolate the relay system from the optical bench. A control Fast Steering Mirror (FSM), designated the CFSM, is used to correct the disturbed beam. The corrected beam is then reflected off the platform to the target Position Sensing Detector (PSD).
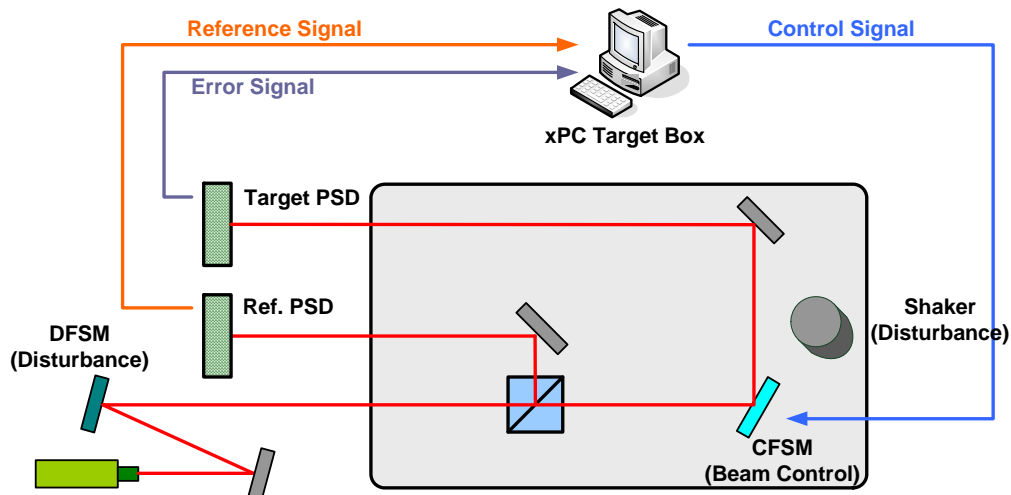
Figure 2. Schematic of the laser jitter control testbed

Fast Steering Mirrors

The Fast Steering Mirrors (FSMs) in the LJC testbed use voice coils to position the mirrors in response to commanded inputs. The LJC testbed uses two different FSMs, one manufactured by the Newport Corporation, and one by Baker Adaptive Optics. The Newport FSM is used as the control mirror (CFSM) for all experiments conducted during this research. The mirror comes with its own controller, the FSM-CD100, capable of both open loop and closed loop operation. The controller also provides an output of the mirror's angular position about each of the axes. In these experiments, the controller is configured in the open loop mode, with control inputs provided from the computer control system. The Newport FSM has a control bandwidth of about 500 Hz.

The second FSM from Baker Adaptive Optics is a one inch diameter mirror used for disturbance injection (DFSM) in these experiments. The Baker mirror comes with a small driver for positioning the mirror; however there is no closed loop option and mirror position is not available.

Position Sensing Detectors

The laser beam optical position sensors, known as Position Sensing Modules or PSMs, were purchased from OnTrak Photonics Inc. and have a detection area of 10mm x 10mm. Each duolateral, dual axis PSM (model PSM2-10) requires an amplifier, the OT-301, to output the x and y position (in volts) of the centroid of the laser beam spot. The combination of amplifier and detector is called a Position Sensing Detector (PSD). The detectors have a minimum sensitivity of 50-100 microwatts, which drives the selection of the beam splitters and the determination of laser power. Their frequency response for the gain settings normally used is 15 kHz. The optimum beam diameter for accurate detection on the PSM is between 1 and 3 mm, and the maximum allowed intensity should be less than 300 W/cm^2. The output range of the PSM2-10/OT-301 detector is ±10 Volts and the OT-301 amplifier has a noise level of 1 millivolt. The minimum resolution of the PSM2-10 with the OT 301 amplifier is 0.5 micrometers.

Newport Vibration Isolation Platform

The CFSM, beam splitters, and folding mirrors are mounted on a bench top pneumatic Newport Vibration Isolation Platform. This platform allows the control system actuators and optical path to be vibrated independent of the optical bench. The breadboard, which is self-leveling, rests on four pneumatic isolators. In order to vibrate the platform at desired frequencies, an inertial actuator is mounted on the vibration isolation platform. This actuator is a CSA model SA-5, capable of delivering a rated force of 5 lbf, in a bandwidth of 20 to 1000 Hz. The SA-5 has a resonance at about 38 Hz. The inertial actuator may be mounted in any orientation. For our experiments, it was mounted next to the last folding mirror before the beam exits the platform, in the vertical direction, to provide maximum x and y axis motion. A separate bracket was designed to allow mounting in the horizontal direction as well. A Kistler model 8690C10 accelerometer is employed to measure the disturbances generated by the inertial actuator on the platform. The accelerometer is driven by a Kistler Piezotron Coupler, model 5124A.

Computer Control System

The computer control system is based on MATLAB, version R2007b with SIMULINK, and the xPC Targetbox, all from Mathworks. The main computer for control implementation and experiment supervision is a 2.4 GHz Dell Dimension 8250 with 1 Gigabyte of RAM. The xPC Target computer has the ability to accept 16 differential inputs and provide 6 analog outputs. The target computer is a Pentium IV running at 2.4 GHz. The disturbance computer, currently controlling the inertial actuator, uses an AMD Athlon processor running at 1.4 GHz, with 256 Megabytes of RAM. dSPACE ver 3.3 with ControlDesk ver 2.1.1 is used to interface with the inertial actuator.

B. Laser Jitter Control Experiments

Laser Jitter Control Algorithms

For laser jitter control, Least Mean Square (LMS), Filtered-X LMS (FXLMS), and Recursive Least Square (RLS) filters were extensively evaluated and improvements were developed in these techniques. The improvement focus was to increase the convergence rate which results in an increased jitter reduction rate. This was done by adding two filters, an Adaptive Bias Filter (ABF) and an Adaptive Phase Filter (APF). A Linear Quadratic Regulator (LQR) was also used in parallel with adaptive filters in some cases.

In adaptive control schemes, the control is determined by adjusting the *tap gains* based on the response of the system to the error, reference signal, and control input. For a LMS method, the tap gain is updated by the following equation

$$\mathbf{w}(n+1) = \mathbf{w}(n) + \mu\mathbf{x}(n)e(n) \tag{1}$$

where $\mathbf{w}$ denotes a tap gain vector, μ is an adaptation rate, $\mathbf{x}(n)$ is signal correlated to the disturbance, and $e(n)$ is an error from the feedback PSD. For the RLS method, the cost function is defined as

$$\xi(n) = \sum_{i=1}^{n} \lambda^{n-1} e^2(i) \tag{2}$$

where λ is a forgetting factor and the error signal at time i is defined as

$$e(i) = d(i) - \mathbf{w}^T(n)\mathbf{x}(i) \tag{3}$$

The optimum weight vector can now be shown as

$$\mathbf{w}(n+1) = \mathbf{w}(n) + \mathbf{k}(n)e(n) \tag{4}$$

where the Kalman gain $\mathbf{k}$ (n) vector is defined as

$$\mathbf{k}(n) = \frac{\lambda^{-1}\mathbf{Q}(n-1)\mathbf{x}(n)}{\lambda^{-1}\mathbf{x}^T(n)\mathbf{Q}(n-1)\mathbf{x}(n)+1} \tag{5}$$

and

$$\mathbf{Q}(n) = \lambda^{-1}\mathbf{Q}(n-1) - \lambda^{-1}\mathbf{k}(n)\mathbf{x}^T(n)\mathbf{Q}(n-1) \tag{6}$$

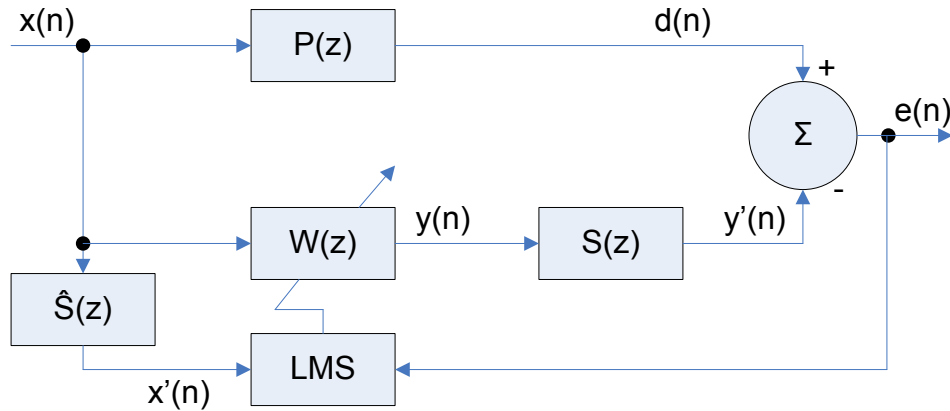Fig 3 shows the block diagram of the Filtered-X LMS (FXLMS) method.

Figure 3. Block diagram of FXLMS method
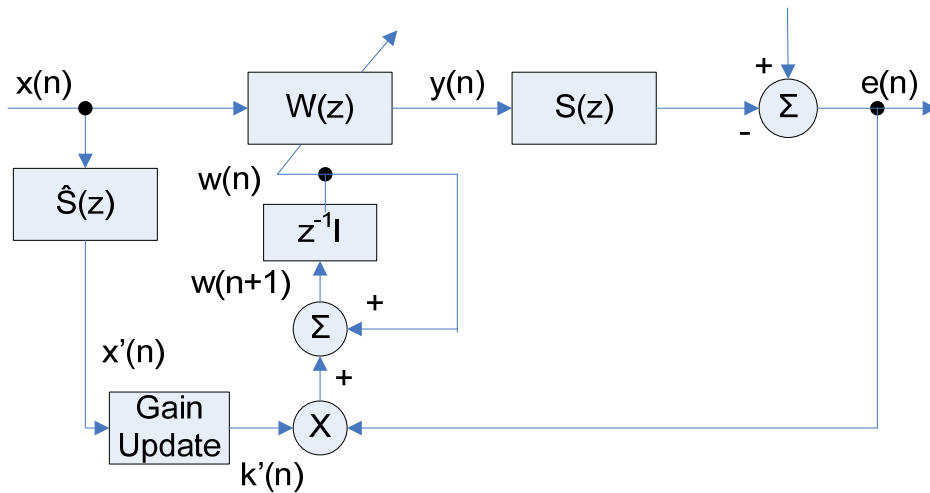
Fig 4 is a block diagram of the Filtered-X RLS method.

Figure 4. Block diagram of FXRLS method

4
American Institute of Aeronautics and Astronautics

Experimental Results

Experiments were performed to verify the control methods including the FXLMS and FXRLS designs. The results of FXLMS and FXRLS methods are compared with LQG control techniques with/without classical notch filters for sinusoidal disturbance rejection. Fig 5 shows the power spectral density of the signal across the frequency spectrum from 0 to 100 Hz.
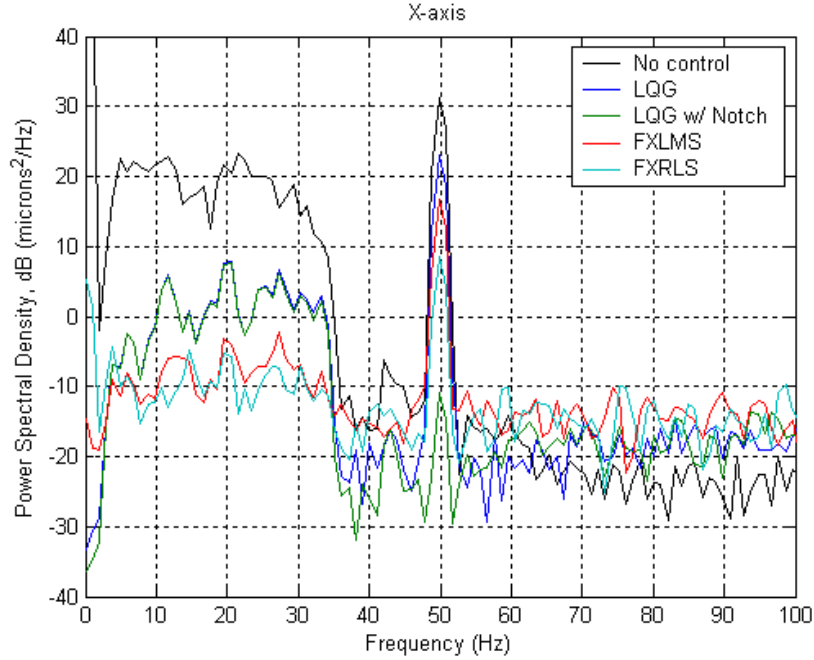

Figure 5. Power spectral density for jitter control methods

The mean squared error plot shown in Fig 6 shows that the FXRLS method manages to further reduce the mean square error of the signal compared to the FXLMS and LQG designs.
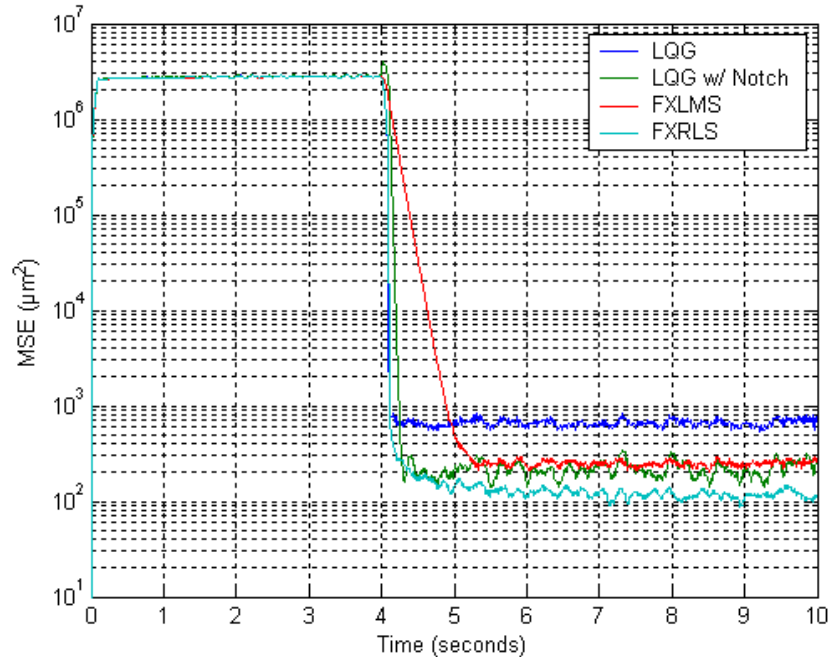
Figure 6. Mean squared error for jitter control methods

A summary of the jitter control results are also presented in Table 1. For the sinusoidal disturbance at 50Hz, LQG with a notch filter provides the best performance. However, to apply this technique, the disturbance frequency must be accurately known and an error or change in disturbance frequency will degrade the performance significantly. Overall FXRLS provides superior performance.

Table 1. Summary of jitter control results

	LQG w/ Notch Filter		FXLMS		FXRLS	
Control Mirror Axis	X axis	Y axis	X axis	Y axis	X axis	Y axis
Input Jitter, st. dev. (µm)	69.5	72.9	69.6	72.5	69.4	72.5
Controlled Jitter, std. dev. (µm)	10.4	11.1	10.4	12.2	6.8	8.4
% Reduction of Jitter	85.1	84.7	85.1	83.2	90.1	88.5
# of Stages	n/a	n/a	1.0	1.0	10.0	10.0
Mean Beam Position Error (nm)	-52.5	162.5	-64.1	-9.6	1591.7	387.1
dB Reduction at 50 Hz	42.1	45.2	14.4	14.1	22.7	33.0
MSE at 10 seconds (µm^2)	249.4		259.8		117.9	

III. Adaptive Optics Control Testbed

The main purpose of an adaptive optics system is to improve the capability of an optical system by actively compensating for wavefront aberrations in real-time. An adaptive optics system consists of a wavefront sensor to measure the aberration of the incoming light, a computer which interprets the sensor data in terms of the aberration profile and control algorithms and a compensation device such as an actuated mirror or electro-optic component. Wavefront compensation will be achieved when the compensation-device applies a conjugate to the phase aberration. Control algorithms are necessary to take into account the imperfect response of the device and to optimize phasing regimes when the wavefront sensor does not provide a means to explicitly calculate the wavefront profile but provides only a means to tell if the level of applied correction has reduced the aberration.
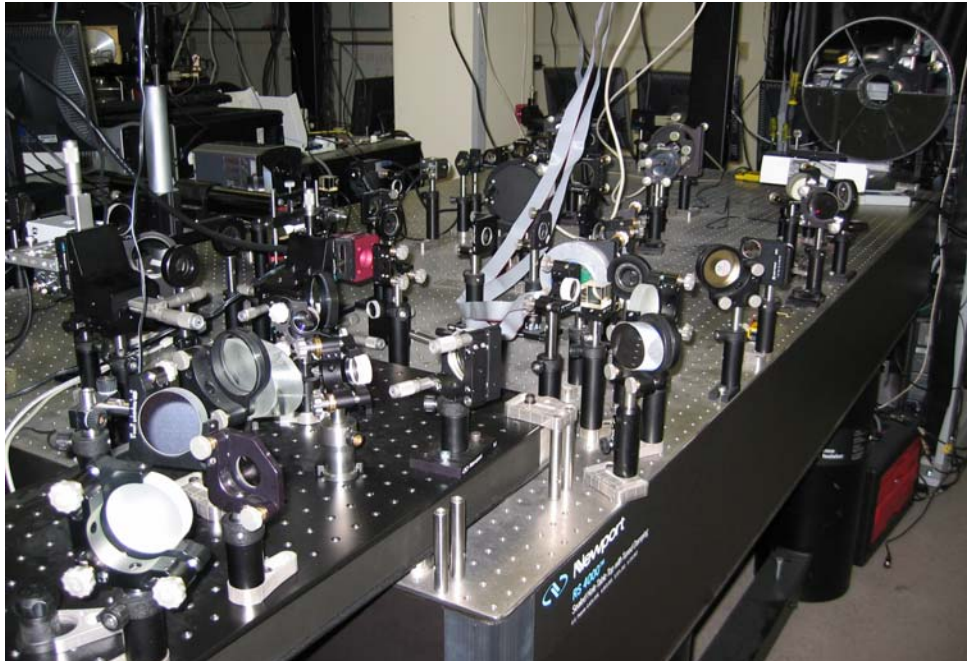
A. Testbed Description
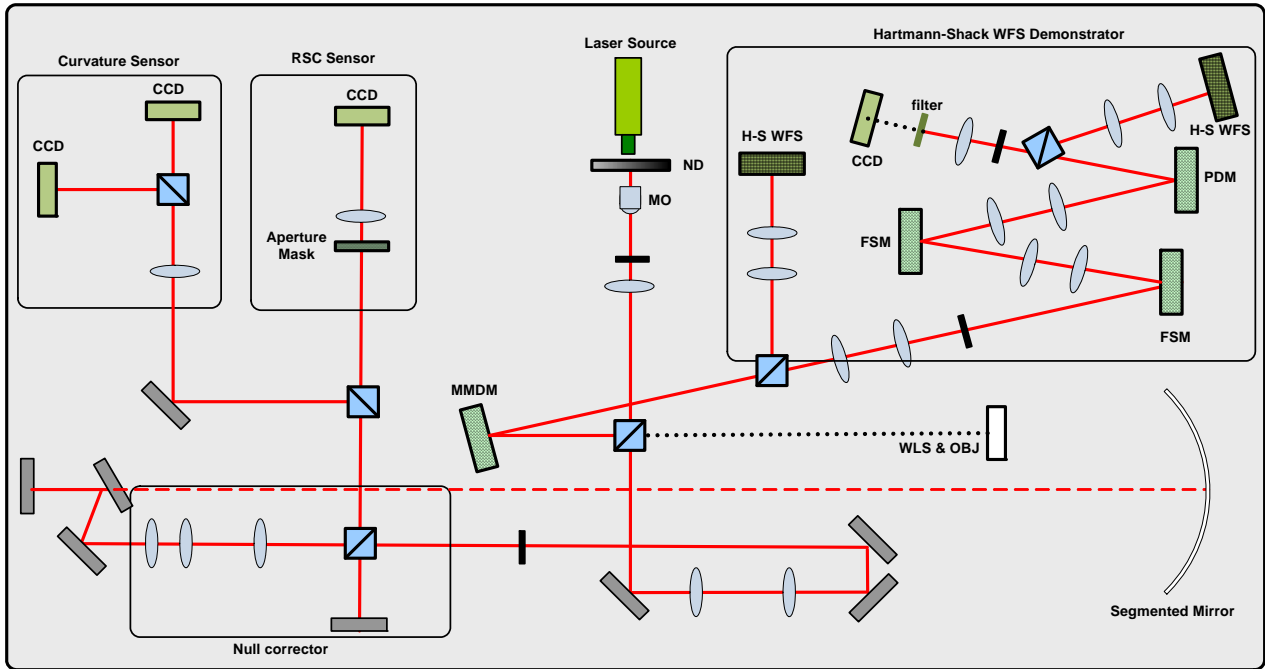
Figure 7. Adaptive optics testbed

Figure 8. Schematic of the adaptive optics control testbed

The current adaptive optics testbed is constructed to test adaptive optics control techniques for large aperture mirrors. The picture of the testbed is shown in Fig 7 and the schematic of the testbed is shown in Fig 8. The testbed employs a segmented mirror representing a deployable telescope mirror in space. When the segmented mirror is deployed in space, it requires accurate alignment between segments. Two wavefront sensors, Phase Diversity and Redundant Spacing Calibration, are used in the testbed for the alignment of mirror segments. In addition to segment misalignment, higher order aberration modes will be present due to deformation of the mirror surface from vibration of moving components onboard the satellite, oscillations of the platform itself as slewing maneuvers are performed, and as rapid thermal changes occur when the aspect changes with respect to the sun. Atmospheric turbulence will not be a source of aberration however, since orbit will be sufficiently high that the atmosphere can be disregarded. For the purpose of calibrating these higher order aberration modes we are using Deformable Mirrors and Shack Hartmann wavefront sensors to provide adequate wavefront sampling. The reference beam is generated on the spacecraft and is used to measure the aberration caused by the primary mirror and the beam jitter onboard the spacecraft. Interference filters and beam splitters are used to isolate the reference beam to measure aberrations caused by the primary mirror surface and jitter. There are three different control loops present for wavefront correction. The primary mirror onboard a spacecraft and in our system will be subjected to some deformation. This deformation will be corrected using a Shack-Hartmann wavefront sensor and the actuators on the first deformable mirror (MMDM in figure 8). The next loop removes the jitter onboard the spacecraft using a fast steering mirror. The jitter is measured using the reference beam and a position sensing detector (Quad Cell). The final loop corrects for any remaining aberrations left in the beam with the other deformable mirror (PDM shown in figure 8). These aberrations may be from external sources as well as internal. The primary mirror actuators will operate at a low frequency because of the large throw required. This means the high frequency disturbances will not be corrected by the actuators on the primary mirror but will be corrected by the second deformable mirror which operates at a higher frequency. The image can be viewed on a monitor while the aberrations are being corrected. Two lenses are used to relay the pupil from the primary mirror to the wavefront sensors to optimize measurement of the aberrations. Similar pairs of doublets are used throughout the testbed to relay the pupil to the various mirrors and sensors used. Each element of the testbed is described in detail as follows.

American Institute of Aeronautics and Astronautics

Segmented Mirror

Carbon fiber segmented telescopes are currently of great interest for space-based imaging since they can be assembled in-situ to deliver a large reflecting area without the bulk and weight of monolithic counterparts. Once assembled, the segments need to be accurately aligned with respect to each other to within a fraction of a wavelength in terms of piston and tip-tilt. This alignment then needs to be maintained as the satellite operates. A 6-segment Carbon fiber mirror measuring 16" in diameter as shown in Figure 9 is used on the adaptive optics testbed and Phase Diversity and Redundant Spacing Calibration techniques are being compared for the calibration of piston and tip-tilt misalignment errors between the segments.

Figure 9. 16 inch Segmented Mirror

Redundant Spacings Calibration

The first method for alignment of the segmented mirror is Redundant Spacings Calibration (RSC). This technique is a Fourier method which uses the image itself as the measurement data and therefore requires no wavefront sensing apparatus, save for an aperture mask. This reduction in optical components is advantageous for space-based platforms. An aperture mask is used to sample spatial frequency components of the wavefront reflecting off the mirror's surface. Redundant (repeated) spacings between apertures provide repeated measurements of the same frequency information at the same instant in time. The discrepancy in these measured quantities provides information about the aberration. The image is Fourier transformed and the phase of each frequency component is found. This can then be used to solve a set of matrix equations yielding piston and tip-tilt phase coefficients of the mirror segments. Alternatively the mirror segments can be phased by optimization of the image sharpness since there is a correspondence between the total intensity of the image and the phase aberration of each spatial frequency component. A control algorithm is used to drive each mirror segment until the position of maximum total image intensity is reached, corresponding to a position of zero phase difference between segments.

Phase Diversity

The second technique, phase diversity, is a well established wavefront sensing method which uses two measurement planes. A separation between these planes is chosen to provide a known phase diversity kernel. The sensor consists of two detectors and a defocusing element. Locally concave regions of the wavefront cause the light to converge as it propagates and locally convex regions of the wavefront cause light to diverge and become less intense (see diagram above right). By measuring the intensity profile at different distances along the propagation

path, diagram, the shape of the wavefront can be estimated. Many algorithms for the wavefront solution exist, some require restrictive assumptions while others are computationally slow. The intensity spot measurement, however, cannot determine whether the rays have a high rate of convergence and have already gone through focus and are now diverging or whether they came from a locally convex region and are slowly diverging. In order to resolve ambiguity the measurement planes need to be brought closer together, thereby limiting dynamic range. It is expected that the RSC sensor will provide greater dynamic range and faster wavefront solution but this is yet to be demonstrated experimentally.

Deformable Mirrors

Two OKO Technologies deformable mirrors are used in the experimental setup, a Mirror Membrane Deformable Mirror (MMDM in Fig 10) and a Piezo-electric Deformable Mirror (PDM in Fig 11). The MMDM is a membrane mirror, with a 5 μm membrane mounted over a two dimensional array of electrodes as shown in Fig 10.
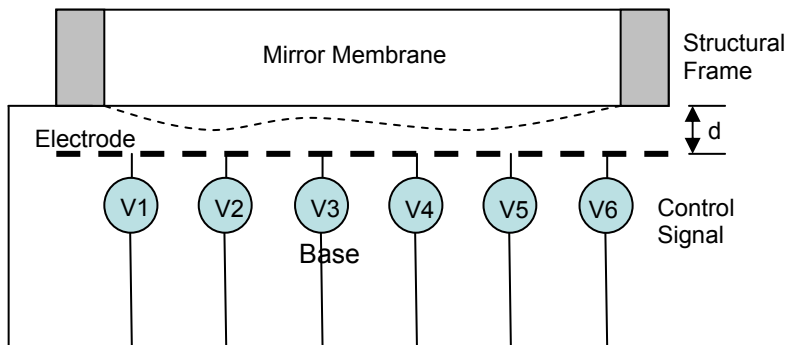

Figure 10.   Mirror Membrane Deformable Mirror (MMDM)

By applying a potential between the electrodes and the membrane, the membrane shape deforms. The mirror has 37 channels (one for each actuator) with 15 mm diameter mirror surface and is built by OKO Technologies.
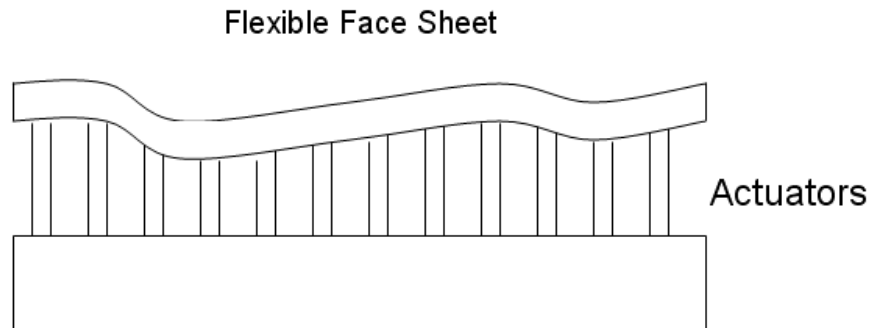

Figure 11.   Simplified Piezo-electric Deformable Mirror Schematic

The Piezo-electric Deformable Mirror (PDM), shown in Fig. 11, is made from a thin solid plate of glass. The plate is bonded to a two dimensional array of piezoelectric actuators. By elongating the piezoelectric actuators, the mirror deforms. The current PDM in the testbed is also built by OKO and has 19 channels and a 30 mm diameter.

Shack-Hartmann Wavefront Sensors

Two Shack-Hartmann wavefront sensors installed on the testbed provide separate closed loop control of the two deformable mirrors. Each Shack-Hartmann wavefront sensor has 127 lenslet elements and is built by OKO Technologies. The principle of the Shack-Hartmann wavefront sensor is shown in Figure 12. The wavefront sensor consists of a lenslet array in front of a CMOS sensor. Each hole on the lenslet array acts as an aperture, and since the source light passing through each lenslet is converging, the image produced on the sensor is an array of spots. The position of the spots in the array is directly proportional to the local wavefront slope at each lenslet. The geometry of the 127 lenslet array used in the testbed is shown in Fig 13.
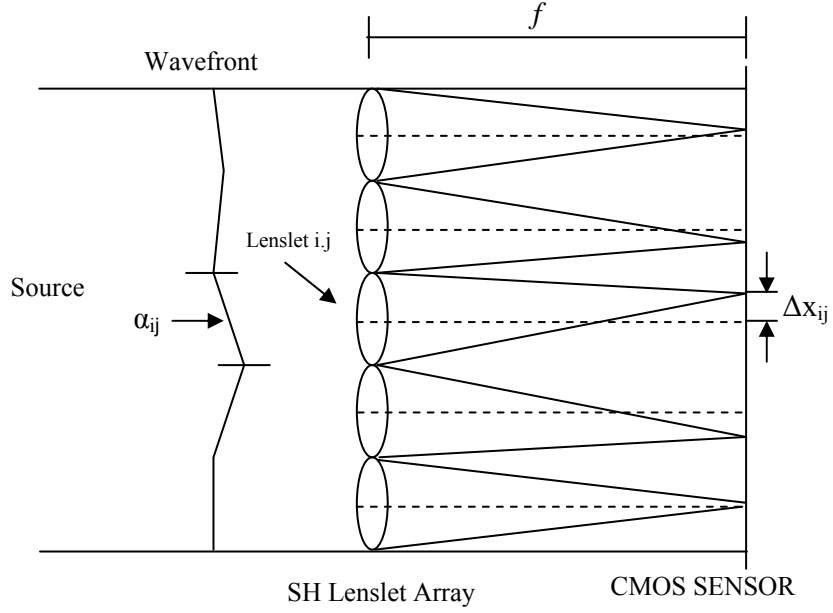
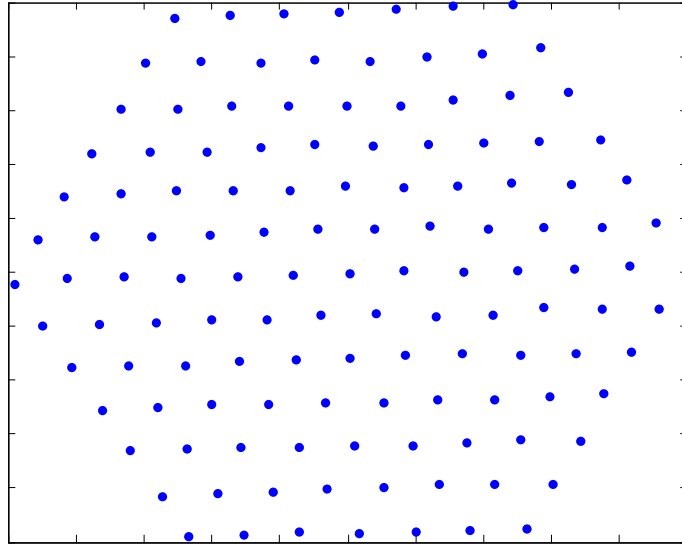**Figure 12.   Shark-Hartmann wavefront sensor principles**

Figure 13.   Shark-Hartmann mask array

B. Adaptive Optics Control Experiments

Wavefront Estimation from Shack-Hartmann Sensors

The local wavefront slopes denoted by α_{ij} and β_{ij} for the x and y directions respectively can be determined by the Shack-Hartmann measurements corresponding to the lateral shifts, Δx_{ij} and Δy_{ij} (Fig 11), of the local focal point on the sensor. Equations (7) and (8) describe this relationship where λ is the wavelength of the reference light source, and f is the focal length of the lenses in the lenslet array[5].

$$\alpha_{ij} = \frac{2\pi}{\lambda f} \Delta x_{ij}, \tag{7}$$

$$\beta_{ij} = \frac{2\pi}{\lambda f} \Delta y_{ij} \tag{8}$$

Optical phase can be represented as a two dimensional surface over the aperture. Deviation from a reference surface is considered the wavefront error. The reference surface used in the experimental work is a planar wavefront. To interpret optical test results it is easy to represent the wavefront as a polynomial series. The polynomial series is shown in Equation (9) where the Zernike coefficients, A_{nm} and B_{nm} , completely describe the wavefront up to the order specified by the largest m and n [6].

$$\phi(r,\theta) = A_{00} + \frac{1}{\sqrt{2}} \sum_{n=2}^{\infty} A_{n0} \Re_n^0 \left(\frac{r}{R} \right) + \sum_{n=1}^{\infty} \sum_{m=1}^{n} \left(A_{nm} \cos(m\theta) + B_{nm} \sin(m\theta) \right) \Re_n^m \left(\frac{r}{R} \right)$$

where,

$$\tag{9}$$

$$\Re_n^0 \left(\frac{r}{R} \right) = \sum_{s=0}^{\frac{n-m}{2}} (-1)^s \frac{(n-s)!}{s! \left(\frac{n+m}{2} - s \right)! \left(\frac{n-m}{2} - s \right)!} \left(\frac{r}{R} \right)^{n-2s}$$

The series is in polar coordinates and the radius, r, is normalized to the unit circle, $\left(\frac{r}{R} \right)$, where R is the aperture radius. Zernike polynomials are orthogonal over the interior of a unit circle, and therefore appropriate for optical surfaces with circular apertures. Zernike polynomials can be transformed to Cartesian coordinates through the relationship, $r = \sqrt{x^2 + y^2}$, and $\theta = \arctan\left(\frac{y}{x} \right)$.

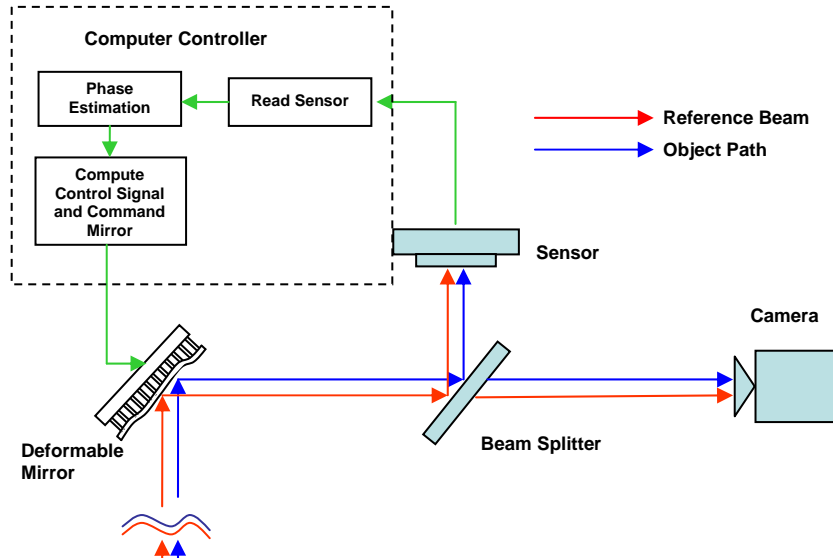*Adaptive Optics Control Methods for MMDM*

Figure 14.   Schematic of wave front correction

The typical adaptive control loop is shown in Fig 14. The reference beam is passing through the same path as the object beam. Deformations of the reference beam will be sensed by the sensor and the deformable mirror will be used to correct the wavefront. Both indirect and direct control approaches were considered in the control design. For the indirect control method, slope data measured by the Shack-Hartmann wavefront sensor is directly

implemented into a feedback control algorithm, avoiding explicit estimation of the phase of the wavefront. The direct control method explicitly reconstructs the phase of a wavefront using either the zonal or the modal method. The reconstructed wavefront is then used to correct the deformation of the wavefront. Two different control methods, an iterative feedback method and a gradient method were initially investigated. For indirect iterative feedback control, the control law becomes

$$c_{n+1} = c_n - gB_s^\dagger s_n \tag{10}$$

where c is a control voltage to the mirror, g is a gain, $B_s^\dagger$ is a pseudo-inverse of a matrix influence matrix B_s, and s_n is the slope measurement from the Shack-Hartmann sensor. The influence matrix, B_s, determines the relationship between the control signal of the deformable mirror and the change in the shape of the deformable mirror. The influence matrix is determined by observing the output of the Shack-Hartmann sensor measurement from poking individual actuators of the deformable mirror. The influence matrix determined from experiments usually results in a badly conditioned matrix, which makes pseudo-inverse computation unreliable. In order to overcome this numerical difficulty, we have developed an indirect iterative feedback control with singularity robust inverse method, which can be written as

$$c_{n+1} = c_n - g\left(\left[B_s^T P B_s + Q\right]^{-1} B_s^T P\right)s_n \tag{11}$$

where P and Q represent positive definite weighting matrices. The singularity robust inverse method tries to minimize the following objective function

$$J = \left(B_s c - s\right)^T P\left(B_s c - s\right) + c^T Q c \tag{12}$$

which is a combined measure of correction error and the magnitude of the control signal. For indirect iterative gradient feedback control, the control signal is generated in the direction where the error of the phase slope measurement is reduced. The total error of the slope measurement is defined as $E = \left[B_s c - s_0\right]^T \left[B_s c - s_0\right]$ where s_0 is the reference slope of the wave front. The partial derivative of the total error becomes

$$\frac{\partial E}{\partial c} = 2B_s^T\left(B_s c - s_0\right) = 2B_s^T\left(s_c - s_0\right) \tag{13}$$

For a flat wavefront, s_0 should be zero, and the indirect gradient control law can be written as

$$c_{n+1} = c_n - 2\mu B^T s_c \tag{14}$$

where μ is a gain of the control loop.

The iterative control and gradient control method can be applied similarly to the direct control problems. The direct control algorithms can use the modal estimates of the coefficients of the Zernike polynomials (a_k). The direct iterative zonal feedback method can be written as

$$c_{n+1} = c_n - gB_\phi^\dagger \phi_n = c_n - g\left[A^\dagger DB\right]^\dagger \phi_n \tag{15}$$

where A is a matrix which relates measured slopes to phase, D is a geometry matrix, and B is an influence matrix. Typically, matrix A was poorly conditioned during experiments, resulting in a poor wavefront estimation. The direct iterative modal feedback control law is written as

$$c_{n+1} = c_n - gB_a a_k = c_n - g\left[dZ^\dagger B_s\right]^\dagger a_k \tag{16}$$

where dZ is determined by the number of Zernike polynomial terms included in the design. The direct gradient feedback control is determined by defining a total error of the wave front represented by the Zernike polynomials.

$$E = \frac{1}{\pi} \int_{-1}^{1} \int_{-\sqrt{1-x^2}}^{\sqrt{1-x^2}} \left[\sum_{k=0}^{M} a_k z_k(x,y) \right]^2 dxdy \tag{17}$$

where $z_k(x,y)$ is a kth Zernike polynomial term. The partial derivative of the total error becomes

$$\frac{\partial E}{\partial c} = 2B^T \left(a * w^2 \right) \tag{18}$$

where $w_k^2 = \frac{1}{\pi} \int_{-1}^{1} \int_{-\sqrt{1-x^2}}^{\sqrt{1-x^2}} \left[z_k(x,y) \right]^2 dxdy$. Then the direct gradient feedback control law becomes

$$c_{n+1} = c_n - 2\mu B^T \left(a * w^2 \right) \tag{19}$$

This method does not require matrix inversion, however the resulting control may yield local minima. In order to improve the performance, we combined the iterative feedback and gradient feedback control such that

$$c_{n+1} = c_n - g B_a^\dagger a - 2\mu B_a^T \left(a * w^2 \right) \tag{20}$$

The flexible dynamics were simulated by injecting a sinusoidal disturbance into the input signal. Second order discrete-time notch filters are considered in the controller which is written as

$$H_z(z) = \frac{1}{2} \left[1 + \frac{k_2 + k_1 (1+k_2) z^{-1} + z^{-2}}{1 + k_1 (1+k_2) z^{-1} + k_2 z^{-2}} \right] \tag{21}$$

where, $k_1 = -\cos(\omega_n)$, $k_2 = \dfrac{1 - \tan\left(\dfrac{BW}{2}\right)}{1 + \tan\left(\dfrac{BW}{2}\right)}$.

Experimental Results

An experiment was performed to correct the wavefront using only the primary deformable mirror and corresponding Shack-Hartmann wavefront sensor. Fig 15 shows the reconstructed wavefront using Zernike polynomials when the primary MMDM is at the neutral bias position. The goal of the experiment is to make the wavefront as flat as possible.
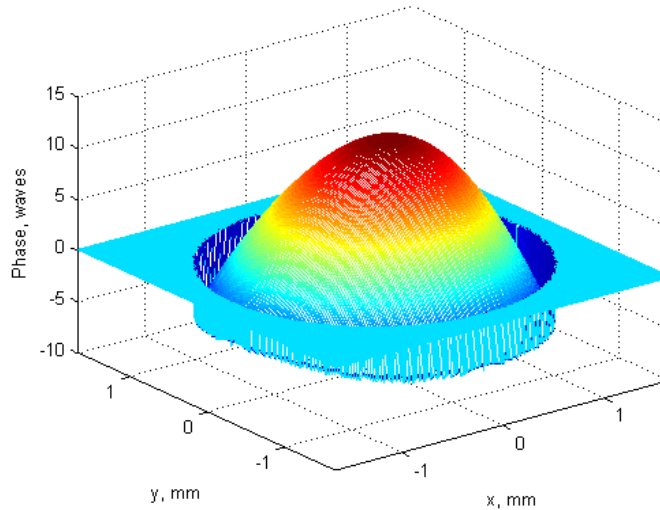

Figure 15.   Shape of wavefront at 127V biased position of MMDM

There could be several measures in evaluating how flat the wavefront is. In our experiments, peak-to-valley and Root-Mean-Squared (RMS) error values over the aperture of the beam are used as qualitative measures. Table 2 summarizes various adaptive optics control results. The results suggest that the combined direct iterative and gradient feedback method provides the best performance for wavefront correction.

Table 2.   Error comparison for wavefront control methods without disturbance

Control Algorithm	Peak to Valley	RMS Wavefront Error
Indirect Iterative Feedback SVD	5.424	2.819
Indirect Iterative Feedback SR	0.266	0.143
Direct Iterative Feedback, Zonal	6.092	2.383
Direct Iterative Feedback, Modal From Zonal	0.268	0.086
Direct Iterative Feedback, Modal from Zernike Derivatives	0.082	0.028
Iterative Gradient Feedback, Variance Minimization	0.736	0.199
Iterative Gradient Feedback, Slope Minimization	0.337	0.089
Combined Direct Iterative and Gradient Feedback	0.022	0.008

An experiment was also performed to investigate the effect of external disturbances. A 5 Hz sinusoidal disturbance is injected to the input signal. With disturbance inputs, the performance of the adaptive optics control techniques significantly degrade as summarized in Table 3.

Table 3.   Error comparison for wavefront control methods subject to a 5 Hz sinusoidal disturbance

	No Disturbance	Disturbance
Control Method	σ	σ_{max} at steady state
Indirect Iterative Feedback SR	0.0176	0.91261
Direct Iterative Feedback, Modal from Zernike Derivatives	0.2317	0.8897
Iterative Gradient Feedback, Variance Minimization	0.10174	1.95
Iterative Gradient Feedback, Slope Minimization	0.0288	1.6483
Combined Direct Iterative and Gradient Feedback	0.00619	0.8547

With the addition of notch filters, it can be seen from Fig 16 that the RMS error can be further reduced. This notch filter design requires the correct knowledge of the frequency content, and it showed improved performance with a known input disturbance.
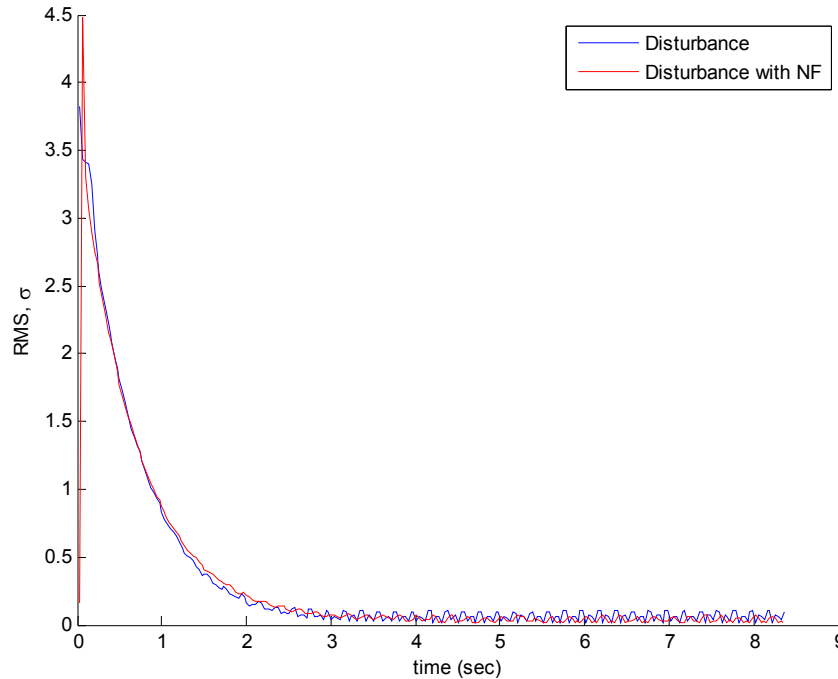
Figure 16. **Error History for 5 Hz Sinusoidal Disturbance** *Amplitude of 54 Volt sinusoidal signal is added on MMDM Actuator 10, with and without Notch Filter. Initial Bias of 127 Volts*

IV. Current and Future Research Work

The current testbed uses a segmented mirror for piston and tip/tilt alignment between mirror segments and deformable mirrors for correction of higher order wavefront aberrations. In the future testbed, each segment of the segmented mirror will have the capability of changing its own shape for correction of higher order wavefront aberrations. Further study on wavefront sensing techniques such as Redundant Spacings Calibration will be performed to include the capabilities of sensing piston and tip/tilt information between segments as well as phase information of the wavefront for higher order aberrations.
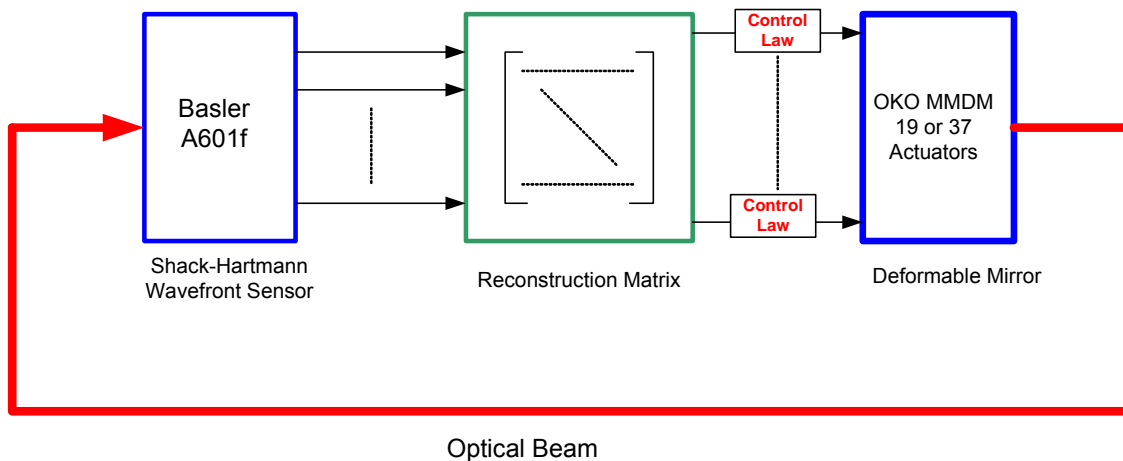

Figure 17. **Adaptive Optics Control Block Diagram**

American Institute of Aeronautics and Astronautics

The control system design for a large segmented mirror is also a challenging problem because of high order and highly coupled system dynamics, flexibility, low damping, and large modeling uncertainties. In addition, for adaptive optics, the number of outputs from wavefront sensors and inputs to deformable mirrors are in the hundreds. As in the adaptive optics control block diagram shown in Figure 17, actuators and sensors are structurally coupled. However, to simplify the design, dynamic coupling is neglected and a Single Input Single Output (SISO) approach is typically used. This simplification results in difficulty in meeting performance because dynamic coupling between the sensors and actuators and between segments is neglected in the control design. Therefore, advanced control techniques including Multi-Input Multi-Output (MIMO) and robust control approaches are necessary to achieve satisfactory control design. One complicating factor of actual systems is the large number of actuator inputs and sensor outputs. The number of inputs and outputs can easily reach to the thousands. Models of systems this large are too computationally complex to design MIMO controllers directly so techniques for model reduction are also required. We are examining model reduction techniques based on singular value decompositions and Zernike polynomials. Future work will focus on using theses control techniques.

V. Conclusion

This paper presents the current optical beam control testbeds at the Naval Postgraduate School and shows operational results of these testbeds. These testbeds are proven effective to demonstrate and evaluate various control techniques for laser jitter control systems and adaptive optics systems. Further upgrades of the testbed will provide an experimental platform for space-based optics systems, especially for testing advanced control techniques for jitter and adaptive optics control for future missions with very challenging requirements. These testbeds will provide confidence in using these techniques in future missions, resulting in improved performance and reduced development time and cost.

Acknowledgements

References

[1] Watkins, R. and Agrawal, B., "The use of an LMS Filter in the Control of Optical Beam Jitter", AIAA Journal of Guidance, Control, and Dynamics, July-August 2007, Vol 30, No.4, pp 116-1122, 2007.

[2] Sugathevan, S. and Agrawal, B. "Optical Laser Pointing and Jitter Suppression using Adaptive and Feedback Control Methods," Proceedings of Beam Control Conference, Directed Energy Professional Society, Monterey, CA, March 21-24, 2006

[2] Dornheim, M. A., "Planetary Flight Surge Faces Budget Realities," *Aviation Week and Space Technology*, Vol. 145, No. 24, 9 Dec. 1996, pp. 44-46.

[3] Yoon, H. and Agrawal, B., "Laser Beam Jitter Control Using Adaptive Filter Technique", Directed Energy Systems Symposium, Beam Control Conference, Monterey, CA, March 2008.

[4] Allen, M., Kim, J. and Agrawal, B., "Control of a Deformable Mirror Subject to Structural Disturbance", SPIE Defense and Security Symposium, Orland, FL, March 2008.

[5] Zhu, L., Sun, P.C., Bartsch, D. U., Freeman, W. R., & Fainman, Y., Adaptive control of a micromachined continuous-membrane deformable mirror for aberration compensation, *Applied Optics*, 38, 168-176., 1999.

[6] Frazier, B. W., & Tyson, R. K., Robust control of an adaptive optics system, *Proceedings of the Thirty-Fourth Southeastern Symposium on System Theory*, 293-296, 2002.